

# Experimental investigation on mechanical properties and permeability evolution of red sandstone after heat treatments\*

Jin YU<sup>†1,2</sup>, Shao-jie CHEN<sup>3</sup>, Xu CHEN<sup>1</sup>, Ya-zhou ZHANG<sup>1</sup>, Yan-yan CAI<sup>1</sup>

<sup>(1)</sup>Institute of Geotechnical Engineering, Huaqiao University, Xiamen 361021, China)

<sup>(2)</sup>State Key Laboratory for Geomechanics and Deep Underground Engineering,  
China University of Mining and Technology, Xuzhou 221008, China)

<sup>(3)</sup>State Key Laboratory of Mine Disaster Prevention and Control, Shandong University of Science and Technology, Qingdao 266510, China)

<sup>†</sup>E-mail: bgyu0717@hqu.edu.cn

Received Dec. 20, 2014; Revision accepted July 27, 2015; Crosschecked Aug. 7, 2015

**Abstract:** Triaxial compression tests were carried out on red sandstone samples which had been previously subjected to heat treatments at 20, 200, 400, and 600 °C to study the change in properties and mechanical characteristics of the rock and the permeability (gas) evolution. Results show that: (1) the color of the sandstone changes from gray to brownish red with incremental change of temperature; (2) the strength of the rock increases with heat treatments from 20 to 200 °C and decreases with heat treatments from 200 to 600 °C, while the permeability of the rock after the heat treatments changes in the opposite trend; (3) from 20 to 200 °C, the primary pores and cracks close gradually, which results in the strength and elastic modulus increasing and permeability of the rock after the heat treatment decreasing; from 200 to 600 °C, the degradation of the sandstone causes the fall in strength and elastic modulus, and the rise in strain corresponding to the peak stress and permeability of the rock after the heat treatment; (4) the permeability in a stress-strain process varies with the evolution of cracks; (5) when the heating temperature is beyond 800 °C, the sandstone is seriously thermally damaged.

**Key words:** Heat treatment, Red sandstone, Triaxial compression test, Mechanical property, Permeability

**doi:**10.1631/jzus.A1400362

**Document code:** A

**CLC number:** TU45

## 1 Introduction

Thermal treatment in rocks produces cracks and alters the crack networks because of the different thermal expansion coefficients of grain minerals. Therefore, it leads to changes in the mechanical and petrophysical properties of rocks (Guéguen and

Schubnel, 2003; Seibt and Kellner, 2003; Fortin *et al.*, 2005; Abdulagatova *et al.*, 2009; Fortin *et al.*, 2011). The evolution of such properties can have either a positive or negative impact on different engineering applications. For example, improving the rock permeability is important for both enhanced oil recovery (Shafiei and Dusseault, 2013) and gas extraction from tight gas reservoirs (Zou *et al.*, 2012). On the other hand, in underground coal gasification (UCG), the cavity zone may have an adverse effect on the stability of the surrounding rock and the gasification products may escape through pre-existing and newly created cracks and, thus, pollute underground water aquifers (Minchener, 2005; Yang *et al.*, 2008; Kapusta *et al.*, 2013). Similarly, in nuclear waste storage sites, temperature induces thermal cracking in the surrounding rocks and thus increases their

\* Project supported by the National Natural Science Foundation of China (Nos. 51374112 and 51474134), the Fujian Provincial Natural Science Foundation of China (No. 2014J01160), the Open Research Fund of State Key Laboratory for Geomechanics and Deep Underground Engineering, China University of Mining and Technology (No. SKLGDUEK1304), and the Promotion Program for Young and Middle-aged Teacher in Science and Technology Research of Huaqiao University (No. ZQN-PY112), China

 ORCID: Jin YU, <http://orcid.org/0000-0003-0088-7652>

© Zhejiang University and Springer-Verlag Berlin Heidelberg 2015

permeability which may lead to nuclear waste leakage (McKinley *et al.*, 2006; Monfared *et al.*, 2011).

A wide range of studies has been carried out to understand the role of thermal loading on the mechanical properties of porous rocks. Wu *et al.* (2005) performed experiments on sandstone specimens being loaded under and after high temperature. Their results demonstrated that the values of the peak-strength, the elastic modulus, and the deformation modulus of the sandstone they studied decreased gradually showing a generally similar variation tendency. Ranjith *et al.* (2012) explored the mechanical response of sandstone and their results demonstrated that the compressive strength and the elastic modulus increased with increasing temperature up to 500 °C and then decreased for higher temperature values. Zuo *et al.* (2012) observed and studied the thermal cracking of sandstone under different temperatures with scanning electron microscope (SEM), and the experimental results indicated that the main mechanisms of the thermal cracking of sandstone were thermal expansion mismatch and thermal expansion anisotropy, and the critical temperature for the initiation and nucleation thermal cracking of sandstone was shown to be about 150 °C. These studies mainly aimed at the rock mechanics properties (strength and deformation parameters) after being subject to high temperature. Although the relationship between permeability and mechanical properties of rocks is of great importance (Brace *et al.*, 1968; Luo *et al.*, 2011), our knowledge is restricted in terms of how these quantities relate to rocks that have been previously subjected to high temperatures. This study focuses on the evolution of permeability (gas) due to deformation occurring in sandstone samples previously subjected to thermal treatment.

## 2 Experimental

### 2.1 Sandstone material and sample preparation

The test material was a sandstone collected from Jiangxi Province, China. It is composed of fine grains with a mean grain size of about 0.12 mm. From X-ray diffraction (XRD) analysis, the minerals in the sandstone specimens are mainly feldspar, quartz, kaolinite, and chlorite, and more detailed compositions of this rock are described in Fig. 1. A rock-drilling machine was used to core samples and a lathe was used to ensure samples' smoothness and verticality. Sand-

stone samples with a diameter of 25 mm and a length of 50 mm were cored from a single block all at the same orientation (vertical to the bedding plane). Density, porosity, and P-wave velocity of the sandstone samples were measured before the thermal treatment and the results are presented in Table 1. In addition, the average permeability of the sandstone samples before the thermal treatment is about  $5.823 \times 10^{-16} \text{ m}^2$ . During thermal loading, samples stayed inside an electric furnace and they were heated at a rate of 10 °C/min (with a temperature control accuracy of  $\pm 1$  °C). Samples remained inside the furnace for 4 h after having reached the desired temperature and then they were cooled to room temperature (while remaining inside the furnace). The low heating rate was applied to ensure that cracking resulted only due to temperature effects. Four temperature groups were used in the test, namely 20, 200, 400, and 600 °C. We originally used five groups, the highest of which was 800 °C, but the samples were seriously damaged after the heat treatment. Thus, we decided to omit this group. Fig. 2 shows photos of the sandstone samples after being heated at high temperatures. At room temperature the sandstone sample was gray, then at 200–600 °C the samples changed from gray to brownish red, and at 800 °C it was ochre. As shown in Fig. 2b, a large number of macroscopic cracks were produced by thermal stress in the sandstone samples after 800 °C, which made them unsuitable for use.

### 2.2 Testing equipment and procedures

Triaxial compression experiments were carried out at a TAW-1000 electro-hydraulic servo controlled testing system, which enables gas permeability measurements under various confining pressure (Fig. 3). The radial and axial displacement transducer maximum ranges were 2 and 4 mm, respectively. Thus,

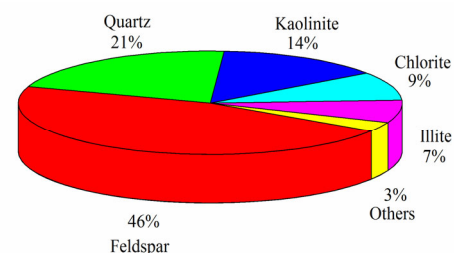
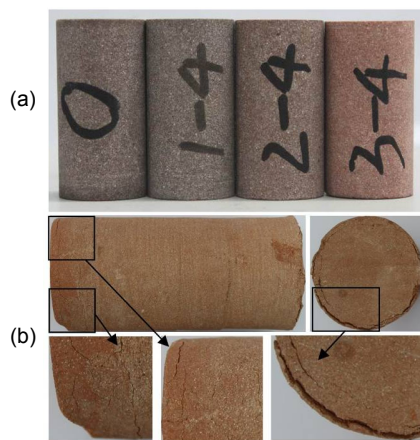


Fig. 1 Mineral composition of sandstone (before heat treatment) derived from XRD

**Table 1 Basic material parameters of tested sandstone samples**

Temperature (°C)	No.	Density				Porosity				P-wave velocity*			
		Value (g/cm <sup>3</sup> )		Growth rate (%)	Average growth rate (%)	Value (%)		Growth rate (%)	Average growth rate (%)	Value (m/s)		Growth rate (%)	Average growth rate (%)
		BH	AH			BH	AH			BH	AH		
20	0-1	2.43	2.43	0		10.18	10.18	0		3459	3459	0	
	0-2	2.44	2.44	0	0	10.23	10.23	0	0	3580	3580	0	0
	0-3	2.43	2.43	0		9.89	9.89	0		3499	3499	0	
	0-4	2.43	2.43	0		10.16	10.16	0		3572	3572	0	
200	1-1	2.43	2.42	-0.41		10.12	11.39	12.55		3407	3322	-2.49	
	1-2	2.41	2.41	0	-0.21	10.03	11.16	11.27	11.31	3490	3287	-5.82	-4.16
	1-3	2.43	2.42	-0.41		10.20	11.25	10.29		3484	3352	-3.79	
	1-4	2.42	2.42	0		10.24	11.38	11.13		3560	3398	-4.55	
400	2-1	2.41	2.40	-0.41		10.26	11.54	12.48		3445	3067	-10.97	
	2-2	2.42	2.40	-0.83	-0.73	9.75	10.96	12.41	12.18	3459	3146	-9.05	-9.3
	2-3	2.42	2.40	-0.83		10.16	11.42	12.40		3523	3215	-8.74	
	2-4	2.41	2.39	-0.83		9.80	10.92	11.43		3484	3190	-8.44	
600	3-1	2.42	2.40	-0.83		9.54	10.97	14.99		3445	2379	-30.94	
	3-2	2.43	2.39	-1.65	-1.24	10.36	11.85	14.38	14.32	3489	2368	-32.13	-31.24
	3-3	2.42	2.38	-1.65		10.05	11.48	14.23		3516	2487	-29.27	
	3-4	2.42	2.40	-0.83		10.54	11.98	13.68		3499	2358	-32.61	

\* P-wave velocity was tested under dry condition; BH: before heat treatment; AH: after heat treatment



**Fig. 2 Sandstone samples after heat treatment**  
 (a) Available samples (20, 200, 400, and 600 °C); (b) Unavailable samples (800 °C)

the initial displacement was controlled as far as possible within 300 and 500 μm. During the experiments, the axial stress, axial and lateral strain of the tested sandstone samples were recorded simultaneously.

The sample was positioned between two steel end-plugs, each of which had a concentric hole at the center for fluid access to the upstream and downstream pore pressure system. The sample and steel end-plug were wrapped with black tape and tightened

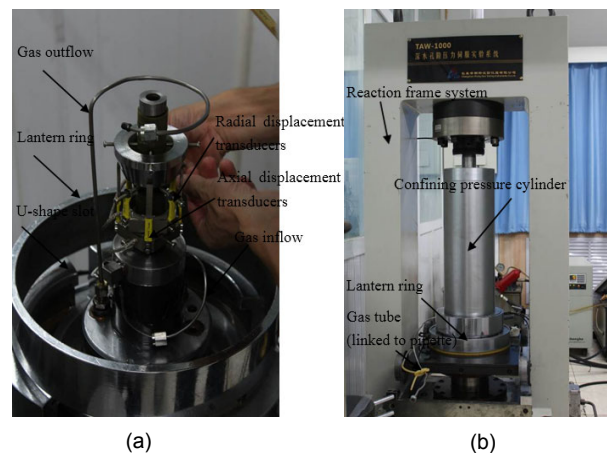


**Fig. 3 Sample assembly (a) and TAW-1000 electro-hydraulic servo controlled testing system (b)**

with heat-shrink pipe to isolate the pore pressure from the confining pressure. Then the axial and radial displacement transducers were installed, and the assembled sample was placed into the chamber on the lower cylinder of the load frame (Fig. 3a). Next the triaxial cell was lowered and filled with oil so that the confining pressure could be applied. During these experiments, we tested different confining pressures:  $P_c=0$  MPa (uniaxial compression), 5, 10, and 20 MPa.

In a triaxial compression test, the confining pressure was loaded to 1 MPa by displacement control at a rate of 20 mm/min. Then the loading method was changed to pressure control at a rate of 6 MPa/min to a desired confining pressure  $P_c$ , and then the axial stress ( $\sigma_1$ ) was increased incrementally at a rate of 0.06 mm/min while the radial stresses ( $\sigma_2=\sigma_3=P_c$ ) remained constant, where  $\sigma_i$  ( $i=1, 2, 3$ ) denote the three principal stresses.

For the measurement of rock permeability, two different experimental techniques were used: the steady-state flow (or permanent regime) method, and pulse test (or transient regime) technique. The choice of the one or the other method mainly depends on the range of permeability to be determined. In general, for materials with relatively high permeability (e.g.,  $>10^{-16}$  m<sup>2</sup>), it is easy to reach the permanent flow regime, and the steady-state flow is preferred (Brace *et al.*, 1968). In the case of the red sandstone samples used here, the initial permeability is relatively high, ranging from  $10^{-16}$  to  $10^{-15}$  m<sup>2</sup>. Thus, the steady-state flow method was chosen and the nitrogen was adopted for the penetrating fluid in this test. One end of the dry sample was connected to a nitrogen gas cylinder and 2.0 MPa pressure was applied to this end. The other end was open to atmospheric pressure. So a 2.0 MPa gas pressure gradient was imposed between these two ends and kept constant, which allowed the fluid to flow from one end of the sample towards the other. In the whole process of triaxial compression, 6–8 points of gas permeability were measured. When the gas valve was open, the gas flowed through the sample and then flowed into the transfer pipette (via previous water wetting). The transfer pipette had inhaled a small amount of water to form a blister in advance. Driven by the gas, the blister could move in the pipette. When the gas permeability was measured, the axial loading was suspended and the gas flow rate could be calculated by recording the distance (i.e., the fluid volume) the blister had moved in the pipette and the corresponding time.

For steady-state gas flow, the permeability was calculated according to Darcy's law (Scheidegger, 1974) for compressive media:

$$K = \frac{2QL\mu P_0}{A(P^2 - P_0^2)}, \quad (1)$$

where  $K$  is the sandstone permeability (m<sup>2</sup>),  $Q$  is the

flow rate of the gas (m<sup>3</sup>/s),  $\mu$  is the nitrogen dynamic viscosity (Pa·s) ( $1.83 \times 10^{-5}$  Pa·s at 20 °C,  $1 \times 10^5$  Pa),  $L$  is the length of the sample (m),  $A$  is the section of the sample (m<sup>2</sup>),  $P_0$  is the atmospheric pressure (Pa), and  $P$  is the injection pressure (Pa).

### 3 Results

#### 3.1 Variations in rock properties after heat treatments

Density, porosity, and ultrasonic velocity are important rock properties and are often used to characterize porous materials. Density was calculated by measuring the weight and the volume (diameter and length) of the samples according to the methods recommended by the International Society of Rock Mechanics (ISRM) (Ulusay and Hudson, 2007). P-wave velocities were calculated by measuring the P-wave arrival times along the length of each sample using a Tektoninix digital phosphor oscilloscope 3012 and two P-wave transducers with a frequency of 0.5 MHz. Porosity was calculated by measuring the volume of the sample and the volume of the rock matrix using a core porosimeter. Table 1 shows the measured values of the above-mentioned properties of the sandstone samples before and after the thermal treatment (no mechanical loading). As shown in Table 1, the density and the P-wave velocity of this sandstone after heat treatment have smaller values than those before heat treatment; however, the porosity has an opposite tendency. In addition, the rates of variation of these three parameters increase with the increase of temperature. Variations in density, porosity, and P-wave velocity due to heat treatment temperature in sandstone (Tian *et al.*, 2012) and other kinds of rocks (e.g., granite, marble, and limestone) were also studied by other researchers (Géraud *et al.*, 1992; Chaki *et al.*, 2008; Sengun, 2014) and their results came to similar conclusions with those above. It is likely that density decrease is caused by the volume expansion after the heat treatment, as was suggested by Wu *et al.* (2003) and Chen *et al.* (2005). The reason for changes in porosity and P-wave depending on heat treatment might be the change of the inner structure of the rock induced by thermally stress, as was measured by Géraud *et al.* (1992) using X-ray computerized tomography.

### 3.2 Stress strain relationship and mechanical parameters of the sandstone samples being subjected to different confining pressures after heat treatments

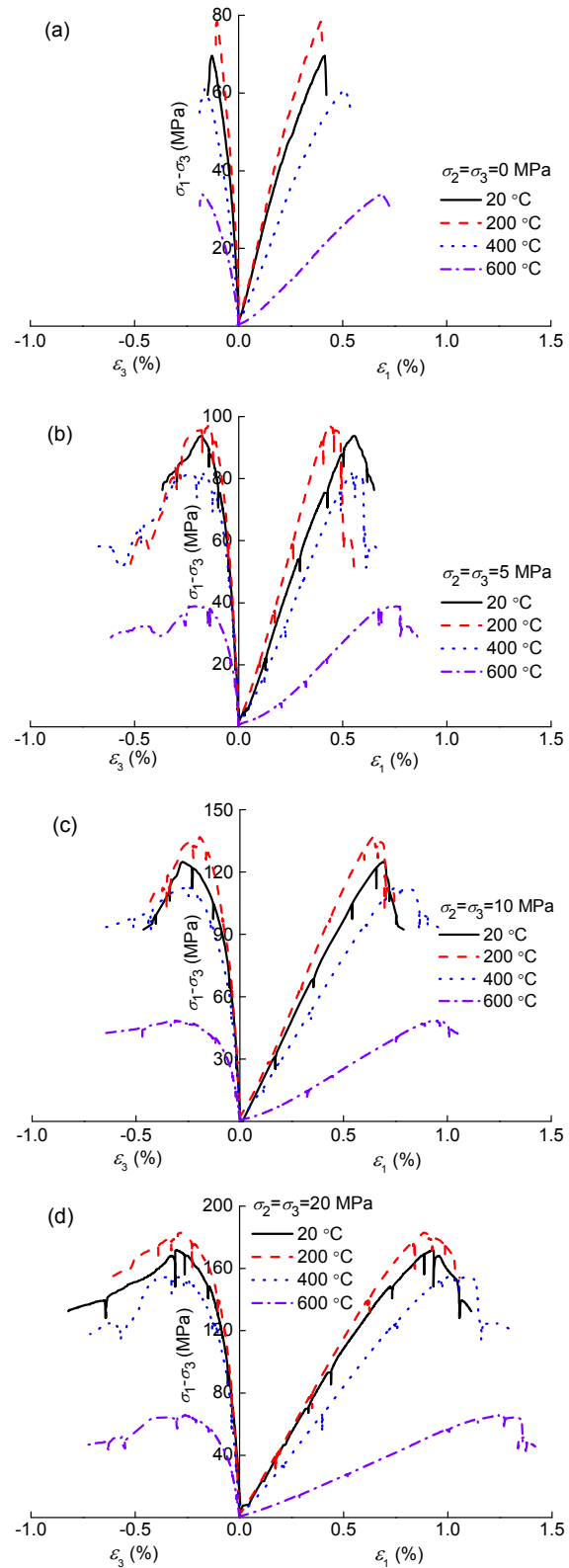
The stress-strain behavior of this sandstone under various confining pressures after heat treatment is shown in Fig. 4. It can be seen from the diagram that, when the sandstone samples are loaded under uniaxial compression (zero confining pressure, Fig. 4a): (1) for heat treatments from 20–200 °C, the strength increases and there is an abrupt stress drop after the peak stress; (2) the strength reduces, ductility increases and shows a slight yield stage before the peak stress from 200 °C to 600 °C; (3) the strength declines significantly (compared to the 200 °C case) after 600 °C. The mechanical behaviour of samples that were loaded under triaxial compression shows differences as compared to that of samples that were subjected to uniaxial compression (Figs. 4b, 4c, and 4d): the yield stage is remarkable before the peak stress, and the length of the yield stage is longer as the confining pressure rises.

Fig. 5 shows the strain values corresponding to the peak strength of sandstone samples being subjected to various confining pressures after different temperature treatments. In Fig. 5a, the peak strength for all tested confining pressures slightly increases from 20 to 200 °C, declines from 200 to 400 °C and declines rapidly from 400 to 600 °C. The equivalent strains decrease slightly from 20 to 200 °C and then increase from 200 to 600 °C.

From the analysis of the uniaxial and triaxial compression tests performed on the sandstone samples, we determined a series of mechanical parameters under various confining pressures after different temperature treatments (Table 2). In Table 2, the Young's modulus  $E$  and Poisson's ratio  $\nu$  were respectively calculated by Eqs. (2) and (3) (Timoshenko and Goodier, 1951), in which the stress and strain values used were corresponding to those values at the half peak stress of the stress-strain curves:

$$E = \frac{(\sigma_1 + \sigma_3)\sigma_1 - 2\sigma_3^2}{(\sigma_1 + \sigma_3)\varepsilon_1 - 2\sigma_3\varepsilon_3}, \quad (2)$$

$$\nu = \frac{\sigma_1\varepsilon_3 - \sigma_3\varepsilon_1}{2\sigma_3\varepsilon_3 - (\sigma_1 + \sigma_3)\varepsilon_1}. \quad (3)$$



**Fig. 4 Stress-strain relationship curves with different confining pressures after heat treatment**  
 (a)  $P_c=0$  MPa; (b)  $P_c=5$  MPa; (c)  $P_c=10$  MPa; (d)  $P_c=20$  MPa;  
 $\varepsilon_1$ : axial strain;  $\varepsilon_3$ : radial strain

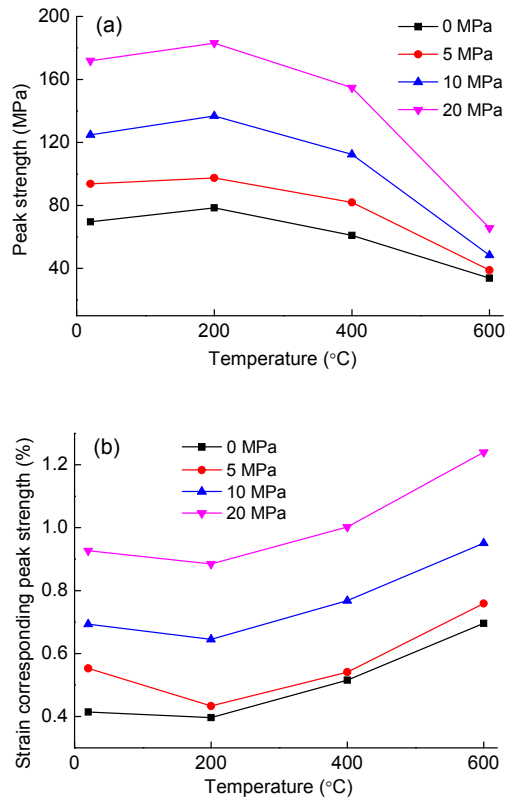


Fig. 5 Peak strength (a) and corresponding strain (b) of sandstone samples under different confining pressures after heat treatment

Fig. 6 shows the Young's modulus and Poisson's ratio after different heat treatments. The results show that the Young's modulus increases from 20 to 200 °C, then decreases from 200 to 600 °C, while the Poisson's ratio does not show any particular trend with

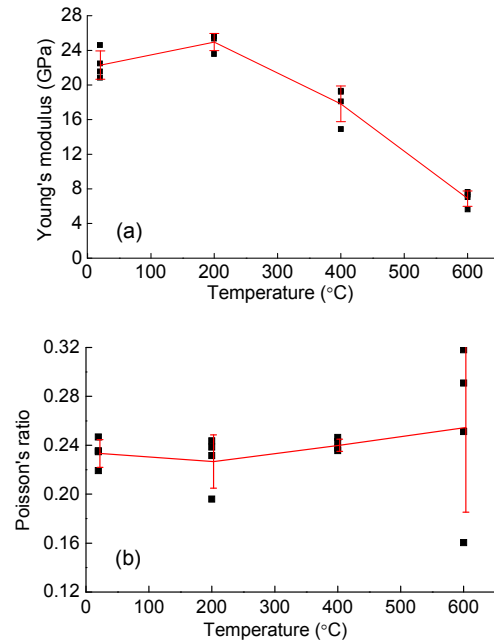


Fig. 6 Young's modulus (a) and Poisson's ratio (b) after heat treatment at different temperatures

Table 2 Strength and deformation values of sandstone samples under triaxial compression tests

Temperature (°C)	No.	Confining stress (MPa)	Peak stress (MPa)	Strain corresponding to the peak stress (%)	Young's modulus, $E$ (GPa)	Poisson's ratio, $\nu$
20	0-1	20	171.92	0.927	24.62	0.247
	0-2	10	124.82	0.693	22.47	0.235
	0-3	5	93.74	0.553	21.56	0.235
	0-4	0	69.61	0.414	20.85	0.219
200	1-1	20	183.05	0.885	25.68	0.239
	1-2	10	136.87	0.645	25.62	0.232
	1-3	5	97.49	0.433	25.34	0.244
	1-4	0	78.40	0.396	23.58	0.196
400	2-1	20	154.78	1.002	19.34	0.246
	2-2	10	112.35	0.766	18.10	0.236
	2-3	5	81.94	0.541	19.21	0.238
	2-4	0	60.98	0.515	14.89	0.243
600	3-1	20	65.64	1.240	6.91	0.318
	3-2	10	48.42	0.951	7.04	0.291
	3-3	5	38.86	0.759	7.64	0.251
	3-4	0	33.90	0.696	5.62	0.160

temperature. Mao *et al.* (2009) worked on limestone samples being subjected to a range of temperatures between room temperature and 800 °C, and showed that the relationship between the modulus of elasticity and temperature variation can be described by a cubic polynomial approximation, which is not in accordance with what we have observed for the equivalent case of sandstone samples. This discrepancy could be explained by the different mineralogical composition of the two rock types.

Fig. 7 shows photographs of the fracture patterns of the sandstone samples after compression testing. The photographs demonstrate the following: (1) At room temperature, with increasing confining pressure, sandstone failure gradually changes from tensile to shear failure (orientation of the fractures). (2) Under uniaxial compression, within the range of 20–200 °C, the fractured pattern is shown as shear failure. The shear angle between the fracture surface and the axial direction of the sample is relatively small, and the sandstone shows axial splitting. In addition, with  $T > 200$  °C, the angle between the fracture surface and the axial direction increases. (3) The rock samples are less fragmented than those that have undergone heat treatment at 400–600 °C. From visual observations of the samples, it appears that both temperature and confining pressure should have some effect on the failure type of this sandstone. Such observation is also supported by Yin *et al.* (2012).

### 3.3 Permeability changes and strain-volumetric curves

Martin (1993) proposed the crack strain model to calculate crack initiation strength, and soon afterward the model was expanded to a wide range of applications (Cai *et al.*, 2004; Shang *et al.*, 2015). In this study, the crack strain model was used to calculate the volumetric strain, and the crack volumetric strain to study the permeability evolution with crack strain, the expressions for which are as follows:

$$\varepsilon_v = \frac{\Delta V}{V} = \varepsilon_{axial} + 2\varepsilon_{lateral}, \quad (4)$$

$$\varepsilon_{ve} = \frac{\Delta V}{V_{elastic}} = \frac{1-2\nu}{E}(\sigma_1 + 2\sigma_3), \quad (5)$$

$$\varepsilon_v = \varepsilon_v - \varepsilon_{ve}, \quad (6)$$

where  $\varepsilon_v$  is the volumetric strain,  $\varepsilon_{axial}$  is the axial strain,  $\varepsilon_{lateral}$  is the lateral strain,  $\varepsilon_{ve}$  is the elastic

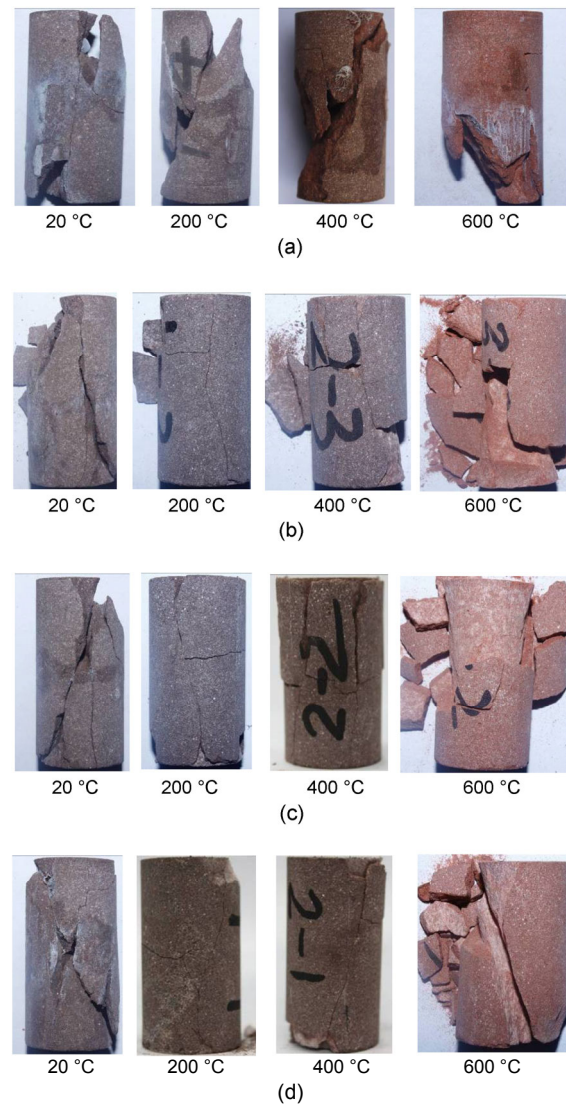


**Fig. 7 Fracture patterns of sandstone samples after compression tests**

(a)  $P_c=0$  MPa; (b)  $P_c=5$  MPa; (c)  $P_c=10$  MPa; (d)  $P_c=20$  MPa

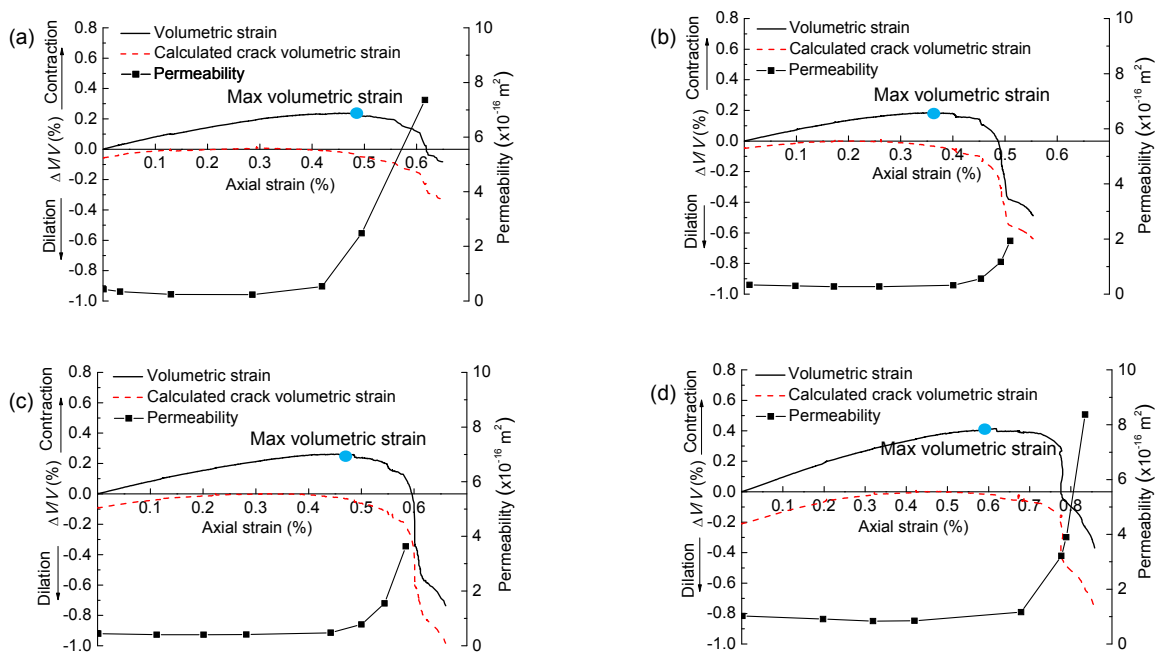
volumetric strain,  $\Delta V$  is the volume change,  $V_{elastic}$  is the elastic volume, and  $\varepsilon_{ve}$  is the crack volumetric strain.

Fig. 8 shows the volumetric strain, crack volumetric strain, and permeability variation as a function of axial strain of the sandstone after heat treatment under 5 MPa confining pressure. A similar variation pattern is also observed in other confining pressure experiments (not shown herein). Fig. 8 demonstrates the following: (1) the maximum volumetric strain (contraction) decreases with temperatures from 20 to 200 °C and increases from 200 to 600 °C; (2) the permeability increases more rapidly during the

deviatoric loading in higher temperature treatment samples (from 200 to 600 °C); (3) during the deviatoric loading, contraction takes place initially followed by dilation at the non-linear stage. This occurs in parallel with crack closure, stabilization, and growth as it is shown by the evolution of the calculated crack volumetric strain. Permeability shows an increasing trend.

The permeability evolution with the stress-strain curve of the sandstone is presented in Fig. 9. According to the stress-strain behavior of a loaded rock sample, Takarli and Prince-Agbodjan (2008) defined these stages as follows: crack closure; linear elastic deformation; crack initiation and stable crack growth; crack damage and unstable crack growth; failure and post-peak behavior (Fig. 9). In this study, the definition was used to analyze the effect of heat treatment on the failure process taking place in sandstone samples. In the stress-strain diagram shown in Fig. 9, the crack closure threshold  $\sigma_{cc}$  is defined as zero calculated crack volumetric strain, the crack initiation threshold  $\sigma_{ci}$  is marked as the point where the stress-strain curve departs from linearity, and the crack damage threshold  $\sigma_{cd}$  corresponds to the most-positive value of volumetric strain. These three stress levels represent important stages in the development of the

macroscopic failure process of intact rock samples. From Fig. 9 the following can be seen: (1) During the initial stage of the deviatoric experiment (stage I, crack closure), the stress-strain response is non-linear. The rock sample gets compacted, and the crack volumetric strain decreases, which indicates that initial cracks close and the permeability of the rock decreases. (2) With increasing axial loading (stage II, linear elastic deformation), the rock continues to compact while the crack volumetric strain and permeability remain constant roughly. (3) As loading continues to increase (stage III, stable crack growth), the volumetric stress reaches a maximum value and the crack volumetric strain increases together with the permeability of the rock. This indicates that the microcrack population starts to increase. (4) Before the stress drop (stage IV, crack damage and unstable crack growth), compactant strain decreases, crack volumetric strain increases together with a significant rise in permeability, which might be linked to a higher number of microcracks. (5) As the axial loading reduces (stage V, failure and post-peak behavior), volumetric dilation in the rock sample begins. The crack volumetric strain reduces while the permeability of the rock soars, which is probably because of irregular macrofracture plane sliding.



**Fig. 8** Strain-volumetric and permeability curves of sandstone after heat treatment under 5 MPa confining pressure (a) 20 °C; (b) 200 °C; (c) 400 °C; (d) 600 °C

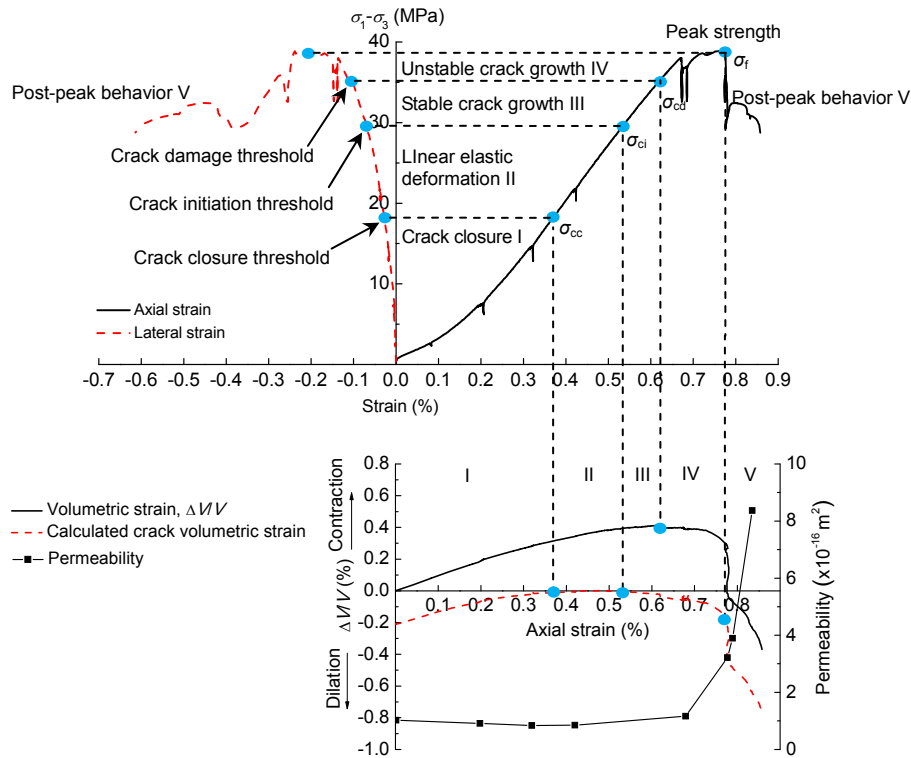


**Fig. 9 Stress-strain relationship and permeability evolution after heat treatment**  
 $\sigma_{ci}$  represents the crack initiation threshold when microfracturing begins;  $\sigma_r$  stands for the peak strength

The data of the initial permeability under various confining pressures after heat treatment are presented in Fig. 10. Under the same confining pressure, it can be seen that: (1) from 20 to 200 °C the initial permeability decreases slightly as the temperature increases; (2) from 200 to 400 °C the initial permeability increases slowly as the temperature increases; (3) from 400 to 600 °C the initial permeability increases quickly as the temperature increases. Under the same treatment temperature: (1) the initial permeability generally decreases as the confining pressure increases, with the exception of 400 °C, which may be due to the randomness of the sandstone’s pore structure; (2) the variance in permeability values is smaller at 200 °C compared with that at 600 °C heat-treated samples.

#### 4 Conclusions

In this paper we investigated the change in the mechanical properties and the evolution of the permeability characteristics in sandstone specimens

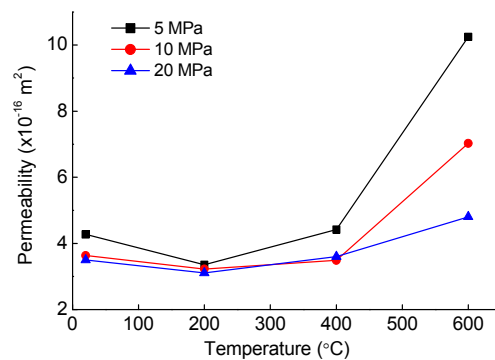


**Fig. 10 Relationship between initial permeability and temperature after heat treatment**

being subjected to different confining pressures ( $P_c=0, 5, 10,$  and  $20 \text{ MPa}$ ) after having undergone heat treatment at 20, 200, 400, and 600 °C. The following conclusions can be drawn:

1. At the temperature of 20–200 °C, the primary pore and cracks gradually closed, which improved the density degree and caused the strength and elastic modulus to increase and permeability to decrease. From 200 to 600 °C, the degradation effects of the

temperature on sandstone became evident, the strength and elastic modulus decreased, and the strain corresponding to the peak stress and initial permeability increased significantly.

2. With the increase of the confining pressure, the degree of internal crack closure in the sandstone increased, which resulted in the reduction of the initial permeability; in addition, larger internal cracks occurred with the severely degraded sandstone samples, which had a greater effect on the closure with the increase of the confining pressure, and the initial permeability decreased more significantly.

3. Gas permeability of sandstone in a complete stress-strain process varied with the evolution of cracks in the samples. In general, the permeability decreased in the initial loading stage due to the crack closure, after which it remained stable in the elastic deformation stage, then gradually increased in the crack growth stage. Prior to the peak strength, the permeability was enhanced sharply by about one or two orders of magnitude.

## References

- Abdulagatova, Z., Abdulagatov, I.M., Emirov, V.N., 2009. Effect of temperature and pressure on the thermal conductivity of sandstone. *International Journal of Rock Mechanics and Mining Sciences*, **46**(6):1055-1071. [doi:10.1016/j.ijrmms.2009.04.011]
- Brace, W.F., Walsh, J.B., Frangos, W.T., 1968. Permeability of granite under high pressure. *Journal of Geophysical Research*, **73**(6):2225-2236. [doi:10.1029/JB073i006p02225]
- Cai, M., Kaiser, P.K., Tasaka, Y., et al., 2004. Generalized crack initiation and crack damage stress thresholds of brittle rock masses near underground excavations. *International Journal of Rock Mechanics and Mining Sciences*, **41**(5):833-847. [doi:10.1016/j.ijrmms.2004.02.001]
- Chaki, S., Takarli, M., Agbodjan, W.P., 2008. Influence of thermal damage on physical properties of a granite rock: porosity, permeability and ultrasonic wave evolutions. *Construction and Building Materials*, **22**(7):1456-1461. [doi:10.1016/j.conbuildmat.2007.04.002]
- Chen, L.J., Zhao, H.B., Gu, H.T., et al., 2005. Study on microstructure of coal roof sandstone under high temperature. *Journal of China University of Mining and Technology*, **34**(4):443-446 (in Chinese).
- Fortin, J., Schubnel, A., Guéguen, Y., 2005. Elastic wave velocities and permeability evolution during compaction of Bleurswiller sandstone. *International Journal of Rock Mechanics and Mining Sciences*, **42**(7-8):873-889. [doi:10.1016/j.ijrmms.2005.05.002]
- Fortin, J., Stanchits, S., Vinciguerra, S., et al., 2011. Influence of thermal and mechanical cracks on permeability and elastic wave velocities in a basalt from Mt. Etna volcano subjected to elevated pressure. *Tectonophysics*, **503**(1-2): 60-74. [doi:10.1016/j.tecto.2010.09.028]
- Géraud, Y., Mazerolle, F., Raynaud, A., 1992. Comparison between connected and overall porosity of thermally stressed granites. *Journal of Structural Geology*, **14**(8-9): 981-990. [doi:10.1016/0191-8141(92)90029-V]
- Guéguen, Y., Schubnel, A., 2003. Elastic wave velocities and permeability of cracked rocks. *Tectonophysics*, **370**(1-4): 163-176. [doi:10.1016/S0040-1951(03)00184-7]
- Kapusta, K., Stańczyk, K., Wiatowski, M., et al., 2013. Environmental aspects of a field-scale underground coal gasification trial in a shallow coal seam at the Experimental Mine Barbara in Poland. *Fuel*, **113**:196-208. [doi:10.1016/j.fuel.2013.05.015]
- Luo, W., Qin, Y.P., Zhang, M.M., et al., 2011. Test study on permeability properties of the sandstone specimen under triaxial stress condition. *Procedia Engineering*, **26**:173-178. [doi:10.1016/j.proeng.2011.11.2156]
- Mao, X.B., Zhang, L.Y., Li, T.Z., et al., 2009. Properties of failure mode and thermal damage for limestone at high temperature. *Mining Science and Technology*, **19**(3): 290-294. [doi:10.1016/S1674-5264(09)60054-5]
- Martin, C.D., 1993. The Strength of Massive Lac du Bonnet Granite around Underground Openings. PhD Thesis, University of Manitoba, Manitoba, Canada.
- McKinley, I.G., Neall, F.B., Kawamura, H., et al., 2006. Geochemical optimisation of a disposal system for high-level radioactive waste. *Journal of Geochemical Exploration*, **90**(1-2):1-8. [doi:10.1016/j.gexplo.2005.09.012]
- Minchener, A.J., 2005. Coal gasification for advanced power generation. *Fuel*, **84**(17):2222-2235. [doi:10.1016/j.fuel.2005.08.035]
- Monfared, M., Delage, P., Sulem, J., et al., 2011. A new hollow cylinder triaxial cell to study the behavior of geo-materials with low permeability. *International Journal of Rock Mechanics and Mining Sciences*, **48**(4): 637-649. [doi:10.1016/j.ijrmms.2011.02.017]
- Ranjith, P.G., Daniel, R.V., Bai, J.C., et al., 2012. Transformation plasticity and the effect of temperature on the mechanical behaviour of Hawkesbury sandstone at atmospheric pressure. *Engineering Geology*, **151**:120-127. [doi:10.1016/j.enggeo.2012.09.007]
- Scheidegger, A.E., 1974. The Physics of Flow through Porous Media. University of Toronto Press, Toronto, Canada, p.102.
- Seibt, P., Kellner, T., 2003. Practical experience in the reinjection of cooled thermal waters back into sandstone reservoirs. *Geothermics*, **32**(4-6):733-741. [doi:10.1016/S0375-6505(03)00071-3]
- Sengun, N., 2014. Influence of thermal damage on the physical and mechanical properties of carbonate rocks. *Arabian Journal of Geosciences*, **7**(12):5543-5551. [doi:10.1007/s12517-013-1177-x]
- Shafiei, A., Dusseault, M.B., 2013. Geomechanics of thermal

- viscous oil production in sandstones. *Journal of Petroleum Science and Engineering*, **103**:121-139. [doi:10.1016/j.petrol.2013.02.001]
- Shang, X.Y., Zhou, G.Q., Lu, Y., 2015. Stress-dependent undrained shear behavior of remolded deep clay in East China. *Journal of Zhejiang University-SCIENCE A (Applied Physics & Engineering)*, **16**(3):171-181. [doi:10.1631/jzus.A1400255]
- Takarli, M., Prince-Agbodjan, W., 2008. Temperature effects on physical properties and mechanical behavior of granite: experimental investigation of material damage. *Journal of ASTM International*, **5**(3):JA1100464.
- Tian, H., Kempka, T., Xu, N.X., et al., 2012. Physical properties of sandstones after high temperature treatment. *Rock Mechanics and Rock Engineering*, **45**(6):1113-1117. [doi:10.1007/s00603-012-0228-z]
- Timoshenko, S., Goodier, J.N., 1951. *Theory of Elasticity*. McGraw-Hill Book Company, New York, USA, p.7.
- Ulusay, R., Hudson, J.A., 2007. The complete ISRM suggested methods for rock characterization, testing and monitoring: 1974-2006. ISRM Turkish National Group, Ankara, Turkey.
- Wu, X.D., Liu, J.R., Qin, J.S., 2003. Effects of thermal treatment on wave velocity as well as porosity and permeability of rock. *Journal of China University of Petroleum (Edition of Natural Sciences)*, **27**(4):70-72 (in Chinese).
- Wu, Z., Qin, B.D., Chen, L.J., et al., 2005. Experimental study on mechanical character of sandstone of the upper plank of coal bed under high temperature. *Chinese Journal of Rock Mechanics and Engineering*, **24**(11):1863-1867 (in Chinese).
- Yang, L.H., Zhang, X., Liu, S.Q., et al., 2008. Field test of large-scale hydrogen manufacturing from underground coal gasification (UCG). *International Journal of Hydrogen Energy*, **33**(4):1275-1285. [doi:10.1016/j.ijhydene.2007.12.055]
- Yin, T.B., Li, X.B., Yin, Z.Q., et al., 2012. Study and comparison of mechanical properties of sandstone under static and dynamic loadings after high temperature. *Chinese Journal of Rock Mechanics and Engineering*, **31**(2):273-279 (in Chinese).
- Zou, C.N., Zhu, R.K., Liu, K.Y., et al., 2012. Tight gas sandstone reservoirs in China: characteristics and recognition criteria. *Journal of Petroleum Science and Engineering*, **88-89**:82-91. [doi:10.1016/j.petrol.2012.02.001]

- Zuo, J.P., Xie, H.P., Zhou, H.W., 2012. Investigation of meso-failure behavior of rock under thermal-mechanical coupled effects based on high temperature SEM. *Science China Physics, Mechanics & Astronomy*, **55**(10):1855-1862. [doi:10.1007/s11433-012-4889-0]

## 中文概要

**题目:** 热处理后红砂岩力学性能及渗透性演化规律三轴试验研究

**目的:** 研究高温热开裂后红砂岩的物理力学性能和渗透性的量化变化规律。

**创新点:** 1. 相比于传统液体稳态流渗透率测试法耗时多的缺点, 本文通过氮气渗透方式, 可快速获得低渗透率岩样的稳态流渗透率; 2. 从裂隙体积变化角度, 分析不同温度热开裂红砂岩在三轴压缩条件下的各裂隙发展阶段, 讨论其与渗透性演化的关系。

**方法:** 1. 通过纵波波速测试和带渗透性实时监测的三轴压缩试验等手段, 获得热处理后红砂岩基本物理力学性质参数(表1和表2)、不同围压下的全应力-应变关系曲线、轴向应变-体变关系曲线以及渗透率变化曲线(图4和图8); 2. 通过理论分析和计算, 获得轴向应变与裂隙体变的关系曲线(图9), 分析裂隙演化5个阶段中渗透率的演化规律。

**结论:** 1. 由20到200 °C, 红砂岩原生孔隙和裂隙发生闭合, 增加了试样密实度, 并引起强度和弹模的提高以及初始渗透率的降低; 从200到600 °C, 红砂岩内部结构逐渐劣化, 导致强度和弹模降低, 峰值应变和初始渗透率提高; 2. 加载过程中试样渗透率随裂隙的演化而变化, 裂隙演化可分为压密、线弹性变形、裂隙稳定发展、宏观剪切破坏和应变软化5个阶段。这5个阶段中渗透率变化趋势不同; 3. 当受热温度继续增大至800 °C时, 红砂岩出现严重的裂纹致使其破坏。

**关键词:** 热处理; 红砂岩; 三轴压缩试验; 力学性能; 渗透性